1984

# Extension of Darby's Model of a Hydrophylic Gas Fed Porous Electrode

Ralph E. White
*University of South Carolina - Columbia*, white@cec.sc.edu

M. A. Nicholson
*Texas A & M University - College Station*

L. G. Kleine
*Texas A & M University - College Station*

J. Van Zee
*Texas A & M University - College Station*

R. Darby
*Texas A & M University - College Station*



## Publication Info

*Journal of the Electrochemical Society*, 1984, pages 268-275.

Publisher's Version: http://dx.doi.org/10.1149/1.2115561
DOI: 10.1149/1.2115561

# Extension of Darby's Model of a Hydrophylic Gas Fed Porous Electrode

R. E. White,* M. A. Nicholson,* L. G. Kleine, J. Van Zee,** and R. Darby

*Department of Chemical Engineering, Texas A&M University, College Station, Texas 77843*

ABSTRACT

A model presented previously by one of the authors (1,2) is reviewed and extended. Aspects of this model which were not previously available in the open literature are considered, and the model is extended to include previously neglected terms in the governing differential equations, fractional reaction orders in the current density-overpotential expression, and mass-transfer coefficients to account for mass-transfer resistance of the reactants to the faces of the porous electrode. The model is used to predict quantities of interest for oxygen reduction in an acidic aqueous solution in a porous carbon electrode.

Many models of gas fed hydrophylic porous electrodes have been proposed as reviewed recently by Chizmadzhev and Chirkov (3) and by Tilak *et al.* (4). Unfortunately, neither of these reviews mentions Darby's model (1, 2) which is based essentially on measurable quantities of the wettable porous electrode of interest and the transport and kinetic properties of the reactants involved. The purpose of this work is to extend Darby's homogeneous model (1) and to present predictions based on this model which include fractional reaction orders and external mass-transfer coefficients for the reactants.

## Homogeneous Model

Darby's (1) homogeneous model is a conceptualization of the chemical, electrochemical, and physical processes that occur within a hydrophylic gas fed porous electrode. Figure 1 schematically presents the representation used here for a region of a gas fed porous electrode which is assumed to be small compared to the dimensions of the electrode. Note that the figure shows the gas pore to be open at both ends, which may be the case in some small volume elements within the electrode; however, the figure does not mean that large gas channels exist from the gas side to the electrolyte side of the electrode. A closer look at Fig. 1 reveals that the gaseous reactant in the pore is assumed to be in local chemical equilibrium with the liquid phase as indicated by $C_{Gi}(z)$, which represents the liquid phase composition of the gaseous reactant at the gas-liquid interface (where a liquid pore intersects a gas pore). Further inspection of Fig. 1 indicates that the concentration of the dissolved gaseous reactant varies with depth ($y$) into the liquid filled pore as indicated by $C_G(y, z)$. Also, note that the coordinate $y$ is normal to the gas-liquid interface and, consequently, is not in the same direction with respect to $z$ for all pores (see Fig. 1 and the List of Symbols).

Once the gaseous reactant has dissolved into the electrolyte at the mouth of a liquid-filled pore, the dissolved gas diffuses into the pore and reacts along the walls of the pore. It is assumed here that no concentration gradient exists across the liquid-filled pore. The flux of the dissolved gaseous reactant ($N_G$) is given by

$$N_G = -D'_{GJ}\frac{dC_G}{dy} + \frac{C_G}{C}(N_G + N_J) \qquad [1]$$

where $J$ represents the liquid phase solvent whose concentration is approximately $C$ and

$$D'_{GJ} = D_{GJ}\frac{\phi_l}{\tau} \qquad [2]$$

($\phi_l$ and $\tau$ will be discussed later). Since $C$ is typically $>> C_G$, Eq. [1] can be simplified to

$$N_G = -D'_{GJ}\frac{dC_G(y,z)}{dy} \qquad [3]$$

The electrochemical reaction that occurs along the pore walls is

$$gG + lL + ne^- \rightleftarrows pP \qquad [4]$$

and the material balance for the dissolved gaseous reactant is

$$\frac{dN_G}{dy} = -\frac{gi'_{os}}{n\mathbf{F}}\left[\left(\frac{C_G(y,z)}{C_{Go}}\right)^{g'}\left(\frac{C_L(z)}{C_{Lo}}\right)^{l'} \exp\left(\alpha\frac{n'\mathbf{F}}{RT}\eta\right)\right] \qquad [5]$$

where cathodic current density and overpotential have been chosen to be positive in order to be consistent with Darby (1, 2). The boundary conditions that apply are as follows

$$\text{at } y = 0 \quad C_G = C_{Gi}(z) \qquad [6]$$

and

$$\text{as } y \to \infty \quad C_G(y,z) = 0, \text{ and } \frac{dC_G}{dy} = 0 \qquad [7]$$

which when applied to Eq. [5] yields

for $g' = 1$

$$C_G = C_{Gi}\exp(-K_1{}^{1/2}y) \qquad [8]$$

and

for $g' \neq 1$

$$C_G(y,z) = C_{Gi}(z)\left\{\frac{g'-1}{2^{1/2}(g'+1)^{1/2}}\xi_1 + 1\right\}^{2/(1-g')} \qquad [9]$$

where

$$\xi_1 = yK_1{}^{1/2}[C_{Gi}(z)]^{(g'-1)/2} \qquad [10]$$

and

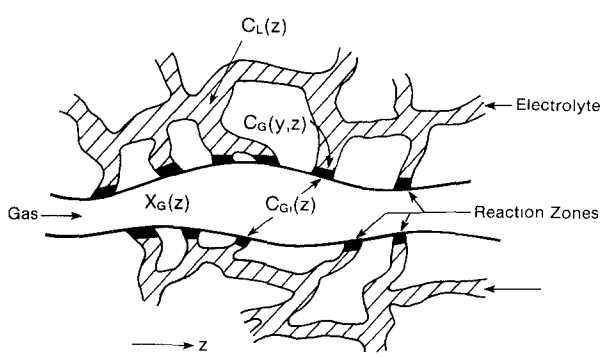


**Fig. 1. Schematic of the homogeneous model for a single gas pore (1).**

* Electrochemical Society Active Member.
** Electrochemical Society Student Member.
Key words: fuel cell, diffusion, mass transport.

$$K_1 = \frac{i'_o sg}{D'_{GJ} n\mathbf{F} C_{Go}{}^{g'}} \left[ \left\{ \frac{C_L(z)}{C_{Lo}} \right\}^{l'} \exp\left\{ \frac{\alpha n'\mathbf{F}}{RT} \eta \right\} \right] \quad [11]$$

It is important to note that Eq. [8] and [9] apply only when the dissolved gaseous species is consumed.

Equation [9] can be used to derive an expression for the rate of consumption of the gaseous reactant per unit of electrode volume ($R_G$)

$$R_G = -a_g D'_{GJ} \frac{dC_G}{dy}\bigg|_{y=0} \quad [12]$$

which by using Eq. [9] becomes

$$R_G = a_g D'_{GJ} \left\{ \frac{2K_1}{g'+1} \right\}^{1/2} [C_{Gi}(z)]^{(g'+1)/2} \quad [13]$$

where $a_g$ is the surface area of the gas-filled pores per unit of electrode volume and will be discussed below.

The dissolved gas that is consumed by the electrochemical reaction must be supplied by diffusion of the gaseous reactant from the electrode/gas interface. This gives rise to the material balance equation for the gaseous reactant within the gas-filled pores

$$\frac{dN_G}{dz} + R_G = 0 \quad [14]$$

The flux of the gaseous reactant ($N_G$) is

$$N_G = -D'_{GI} \frac{P_o}{RT} \frac{dX_G}{dz} + X_G(N_G + N_I) \quad [15]$$

where

$$X_G = P_G/P_o \quad [16]$$

and

$$D'_{GI} = D_{GI} \frac{\phi_g}{\tau} \quad [17]$$

($\phi_g$ will be discussed presently). Since $N_I = 0$ ($I$ represents $N_2$ typically), Eq. [15] can be simplified to

$$N_G = -\frac{P_o D'_{GI}}{RT(1 - X_G)} \frac{dX_G}{dz} \quad [18]$$

Substitution of Eq. [13] and [18] into Eq. [14] and letting

$$\zeta = z/d \quad [19]$$

yields

$$\frac{d}{d\zeta} \left\{ \frac{D'_{GI} P_o}{(1-X)RT} \frac{dX_G}{d\zeta} \right\} = d^2 a_g D'_{GJ} \left\{ \frac{2K_1}{g'+1} \right\}^{1/2} [C_{Gi}(z)]^{(g'+1)/2} \quad [20]$$

Equation [20] can be simplified by using Eq. [11] for $K_1$, Henry's law for $C_{Gi}(z)$ and $C_{Go}$

$$C_{Gi}(z) = X_{Gi}(z) \frac{CP_o}{H} \quad [21]$$

where at $z = 0$ (for no mass-transfer resistance to the electrode from the bulk gas)

$$C_{Go} = C_{Gi}\ (z = 0) = X_{Go} \frac{CP_o}{H} \quad [22]$$

and the definition of the mol fraction of the liquid reactant ($X_L$)

$$X_L = C_L(z)/C \quad [23]$$

and its value at the electrode/electrolyte interface at $z = d$ (for no mass-transfer resistance to the electrode from the bulk electrolyte)

$$X_{Lo} = C_{Lo}/C = C_L\ (z = d)/C \quad [24]$$

When mass-transfer resistance occurs, $X_{Go}$ still represents the mol fraction of the gaseous reactant in the bulk gas, but $X_G(\zeta = 0)$ is no longer equal to $X_{Go}$ and similarly for $X_L(\zeta = 1.0)$ and $X_{Lo}$. Since $X_G = X_{Gi}$, substitution of Eq. [21]-[24] into Eq. [20] yields

$$\frac{d}{d\zeta} \left\{ \frac{1}{1 - X_G} \frac{dX_G}{d\zeta} \right\} = K_G X_G{}^{(g'+1)/2} X_L{}^{l'/2} \quad [25]$$

where

$$K_G = \frac{a_g d^2 RT}{D'_{GI}(g'+1)^{1/2}} \left\{ \frac{2i'_o sgD'_{GJ}C}{n\mathbf{F}P_o H X^{g'}{}_{Go} X^{l'}{}_{Lo}} \right\}^{1/2} \left\{ \exp\left\{ \alpha \frac{n'\mathbf{F}}{RT} \eta \right\} \right\}^{1/2} \quad [26]$$

A similar equation can be derived for the mol fraction of the liquid reactant. The starting point is a flux expression for the liquid phase reactant

$$N_L = -CD'_{LJ} \frac{dX_L}{dz} + X_L(N_L + N_J) \quad [27]$$

where

$$D'_{LJ} = D_{LJ}\, \phi_l/\tau \quad [28]$$

$N_J$ and $N_L$ are often related in a simple manner through the stoichiometry of the electrochemical reaction. For the case considered here, the electrochemical reaction is

$$O_2 + 4H^+ + 4e^- \rightarrow 2H_2O \quad [29]$$

in an aqueous solution.[1] Thus, $J$ is $H_2O$ and $H^+$ is the liquid reactant $L$. Then, according to Eq. [29], the flux of $J$ is related simply to the flux of $L$

$$N_J = -\frac{1}{2} N_L \quad [30]$$

which when substituted into Eq. [27] yields

$$N_L = \frac{-CD'_{LJ}}{1 - \frac{X_L}{2}} \frac{dX_L}{dz} \quad [31]$$

Equation [4] (or [29]) shows that the rate of consumption of the liquid reactant is related simply to the rate of consumption of the dissolved gaseous reactant

$$R_L = \frac{l}{g} R_G \quad [32]$$

The liquid phase reactant must be supplied from the bulk electrolyte as described by the material balance equation for $L$

$$\frac{dN_L}{dz} + R_L = 0 \quad [33]$$

Substitution and simplification as before yields

$$\frac{d}{d\zeta} \left( \frac{1}{1 - \frac{X_L}{2}} \frac{dX_L}{d\zeta} \right) = K_L X_G{}^{(g'+1)/2} X_L{}^{l'/2} \quad [34]$$

where

$$K_L = \frac{a_g l d^2}{D'_{LJ}(g'+1)^{1/2}} \left\{ \frac{2i'_o sD'_{GJ}P_o}{gn\mathbf{F}CHX^{g'}{}_{Go}X^{l'}{}_{Lo}} \right\}^{1/2} \exp\left\{ \frac{\alpha n'\mathbf{F}}{2RT} \eta \right\} \quad [35]$$

Equations [25] and [34] are the governing equations for the mol fractions of the gaseous reactant within the gas-filled pores ($X_G$) and of the liquid reactant within the liquid-filled pores ($X_L$). The boundary con-

[1] It should be noted that in systems operating above the boiling point of the electrolyte the water produced in Eq. [29] would evaporate and leave the cell via the gas phase.

ditions for these equations are as follows

at $\zeta = 0$

$$\frac{dX_L}{d\zeta} = 0 \quad [36]$$

$$k_{mg}[X_G(\zeta = 0) - X_{Go}] = -\frac{D'_{GI}}{d}\frac{dX_G}{d\zeta} \quad [37]$$

and

at $\zeta = 1$

$$\frac{dX_G}{d\zeta} = 0 \quad [38]$$

$$k_{ml}[X_L(\zeta = 1) - X_{Lo}] = \frac{D'_{LJ}}{d}\frac{dX_L}{d\zeta} \quad [39]$$

where $k_{mg}$ and $k_{ml}$ are external mass-transfer coefficients. (Note that when both $k_{mg}$ and $k_{ml}$ become infinitely large, Darby's original boundary conditions are obtained.) Values for $k_{mg}$ and $k_{ml}$ can be predicted for simple systems such as flow between flat plates [see Ref. (5), *e.g.*,] and can be determined experimentally for more complicated systems.

Before proceeding with a solution of the governing equations for $X_G(\zeta)$ and $X_L(\zeta)$, let us consider the distribution of the porosity of the electrode between the gas and liquid pores. The differential pressure ($P = P_o - 1$ atm) determines the fraction of the porosity ($\phi$) filled with gas ($\phi_g$) and the fraction filled with liquid ($\phi_l$) by assuming that the radius of the largest flooded pore is

$$r_e = \frac{2\gamma \cos\theta}{P} \quad [40]$$

Equation [40] states that the gas pressure in the gas-filled pores is balanced by the surface tension of the liquid in the flooded pores. If we assume that the pores wet easily, all pores larger than $r_e$ will be gas-filled and all pores smaller than $r_e$ will be flooded. A cumulative pore size distribution function [$f(r_e)$] can be defined as the fraction of the total pore volume which has pore radii greater than $r_e$

$$f(r_e) = \int_{r_e}^{\infty} \alpha(r)\,dr \quad [41]$$

where $\alpha(r)$ is the pore size distribution function and is assumed here to be normal

$$\alpha(r) = \frac{1}{\sigma\sqrt{\pi 2}} \exp\left[-\frac{1}{2}\left(\frac{r - \bar{r}}{\sigma}\right)^2\right] \quad [42]$$

where $\bar{r}$ and $\sigma$ represent the mean pore radius and the standard deviation of the distribution, respectively. Substitution of Eq. [42] into Eq. [41] yields

$$f(r_e) = \int_{r_e}^{\infty} \left\{ \frac{1}{\sigma\sqrt{\pi 2}} \exp\left[-\frac{1}{2}\left(\frac{r - \bar{r}}{\sigma}\right)^2\right] \right\} dr \quad [43]$$

which can be rewritten in a more convenient form by first breaking the integral into two parts

$$f(r_e) = \int_{o}^{\infty} \left\{ \frac{1}{\sigma\sqrt{\pi 2}} \exp\left[-\frac{1}{2}\left(\frac{r - \bar{r}}{\sigma}\right)^2\right] \right\} dr - \int_{o}^{r_e} \left\{ \frac{1}{\sigma\sqrt{\pi 2}} \exp\left[-\frac{1}{2}\left(\frac{r - \bar{r}}{\sigma}\right)^2\right] \right\} dr \quad [44]$$

and by defining a dimensionless pore radius $r'$

$$r' = \frac{1}{\sqrt{2}}\frac{r - \bar{r}}{\sigma} \quad [45]$$

Then, in terms of $r'$ Eq. [44] becomes

$$f(r'_e) = \int_{o}^{\infty} \frac{1}{\sigma\sqrt{\pi 2}} \exp(-r'^2)\sigma\sqrt{2}\,dr' - \frac{1}{\sigma\sqrt{\pi 2}} \int_{o}^{r'_e} \exp(-r'^2)\sigma\sqrt{2}\,dr' \quad [46]$$

or

$$f(r'_e) = \frac{1}{2} - \frac{1}{\sqrt{\pi}} \int_{o}^{r'_e} \exp(-r'^2)\,dr' \quad [47]$$

which simplifies to

$$f(r'_e) = [1 - \text{erf}(r'_e)]/2 \quad [48]$$

Thus, the fraction of the porosity filled with gas ($\phi_g$) is simply

$$\phi_g = \phi f(r'_e) \quad [49]$$

and the fraction filled with liquid ($\phi_l$) is

$$\phi_l = \phi - \phi_g \quad [50]$$

Both $\phi_g/\tau$ and $\phi_l/\tau$ are used to modify the free stream diffusion coefficients (see Eq. [2] and [17]). The value used here for $\tau$ was chosen arbitrarily. (It may be possible to determine a value for $\tau$ by measuring both $\phi$ and $D'_{GJ}$.)

The porosity ($\phi$), gas phase porosity ($\phi_g$), and the BET-type specific surface area ($a$) can be used to determine an expression for the surface area of the gas-filled pores per unit of electrode volume ($a_g$).

The desired expression for $a_g$ can be obtained by assuming that the pores are tortuous cylinders with a mean pore radius of $\bar{r}$ and by considering the ratio of $a$ to $\phi$

$$\frac{a}{\phi} = \frac{\dfrac{\text{pore wall surface area}}{\text{electrode volume}}}{\dfrac{\text{pore volume}}{\text{electrode volume}}} = \frac{2\pi\bar{r}\tau d}{\pi\bar{r}^2\tau d} = \frac{2}{\bar{r}} \quad [51]$$

or

$$\frac{a}{\phi}\bar{r} = 2 \quad [52]$$

(or some other constant). If Eq. [52] is true for the electrode as a whole, then it is reasonable to assume that it is also true for the gas-filled pores

$$\frac{a_g}{\phi_g}\bar{r}_g = 2 = \frac{a}{\phi}\bar{r} \quad [53]$$

where $\bar{r}_g$ is the mean pore radius of the gas-filled pores which can be normalized in a manner similar to $r_e$

$$\bar{r}'_g = \frac{1}{\sqrt{2}}\frac{\bar{r}_g - \bar{r}}{\sigma} \quad [54]$$

Expressions for $\bar{r}_g$ and then $a_g$ can be obtained in terms of the pore size distribution parameters ($\bar{r}$, $\sigma$) as follows. Since $\bar{r}'_g$ is defined to be the normalized pore radius such that one-half of the gas pore volume is contained in pores with radii larger than $\bar{r}'_g$, the cumulative pore size distribution function $f(\bar{r}'_g)$ is simply one-half of the cumulative pore size distribution for the gas-filled pores [$f(r'_e)$]

$$f(\bar{r}'_g) = f(r'_e)/2 \quad [55]$$

An expression for $\bar{r}'_g$ can be obtained from Eq. [55] by using an equation for $f(\bar{r}'_g)$ which is analogous to Eq. [48] for $f(r'_e)$

$$[1 - \text{erf}(\bar{r}'_g)]/2 = f(r'_e)/2 \quad [56]$$

which can be rearranged to

$$\text{erf}(\bar{r}'_g) = 1 - f(r'_e) \quad [57]$$

or

$$\bar{r}'_g = \text{erf}^{-1}[1 - f(r'_e)] \quad [58]$$

Then according to Eq. [49] and [50], Eq. [58] can be written as

$$\bar{r}_g = \text{erf}^{-1}(\phi_l/\phi) \quad [59]$$

which when combined with Eq. [54] yields an expression for $\bar{r}_g$

$$\bar{r}_g = \bar{r} + \sqrt{2}\,\sigma\,\text{erf}^{-1}(\phi_l/\phi) \quad [60]$$

Substitution of Eq. [60] into Eq. [53] yields

$$a_g = \frac{a\bar{r}\phi_g/\phi}{\bar{r} + \sqrt{2}\,\sigma\,\text{erf}^{-1}(\phi_l/\phi)} \quad [61]$$

which, by using Eq. [48]-[50], becomes the desired expression for $a_g$

$$a_g = \frac{a\bar{r}(1 - \text{erf}\,r'_e)}{2\{\bar{r} + \sqrt{2}\,\sigma\,\text{erf}^{-1}[(1 + \text{erf}\,r'_e)/2]\}} \quad [62]$$

Figure 2 shows the dependence of $a_g$ on the difference between the gas pressure and the electrolyte pressure ($P$). As shown in Fig. 2, $a_g$ is very sensitive to $P$ from about 7 to 12 psi.

## Results and Discussion

The apparent current density (total current/projected area of the electrode) of the porous electrode can be determined from the flux of the gaseous reactant into the porous electrode

$$\frac{gi}{n\mathbf{F}} = N_G|_{\zeta=0} \quad [63]$$

which by using Eq. [18] becomes

$$i = \frac{K_A}{1 - X_G}\frac{dX_G}{d\zeta}\bigg|_{\zeta=0} \quad [64]$$

where

$$K_A = \frac{n\mathbf{F}P_o D'_{GI}}{gdRT} \quad [65]$$

The gradient of the mol fraction of the gaseous species $(dX_G/d\zeta)$ needed in Eq. [64] can be determined from $X_G(\zeta)$ which can be obtained by solving Eq. [25] and [34] subject to the boundary conditions given by Eq. [36]-[39]. Darby (1) found $X_G(\zeta)$ [and $X_L(\zeta)$] by assuming that $X_G$ and $X_L \ll 1$ so that the governing equations for $X_G$ and $X_L$ become

$$\frac{d^2X_G}{d\zeta^2} = K_G X_G^{(g'+1)/2} X_L^{l'/2} \quad [66]$$

$$\frac{d^2X_L}{d\zeta^2} = K_L X_G^{(g'+1)/2} X_L^{l'/2} \quad [67]$$

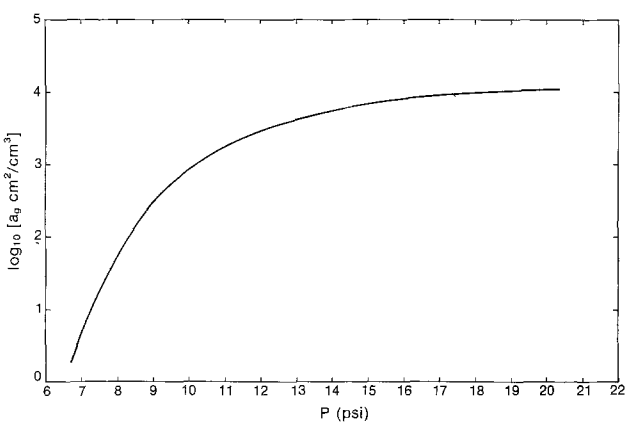


**Fig. 2. Dependence of the surface area of the gas pores per unit of electrode volume ($a_g$) on the differential pressure across the electrode ($P$).**

According to Sepa *et al.* (6), $g' = 1$ and $l' = 1$ or 1.5 for reaction [29] depending on the overpotential. Darby (2) solved approximately Eq. [66] and [67] for $g' = 1$ and $l' = 1$ by assuming that

$$X_G = X_{Go}\left[1 - b\left(\zeta - \frac{\zeta^2}{2}\right)\right] \quad [68]$$

and

$$X_L = X_{Lo}[a' + (1 - a')\zeta^2] \quad [69]$$

which satisfy the boundary conditions (Eq. [36]-[39]) for infinitely large external mass-transfer coefficients and by substituting Eq. [68] and [69] into Eq. [66] and [67] and evaluating the result at $\zeta = 0$ to determine $a'$ and $b$

$$a' = 1 + \frac{K_L^2 X_{Go}^2}{8X_{Lo}} - \left[\left(1 + \frac{K_L^2 X_{Go}^2}{8X_{Lo}}\right)^2 - 1\right]^{1/2} \quad [70]$$

$$b = K_G(X_{Lo}a')^{1/2} \quad [71]$$

Finally, application of Eq. [64] gives the desired expression for the current density

$$i = X_{Go}K_A b \quad [72]$$

Again, Eq. [72] is based on the assumption that $X_G$ and $X_L$ are both much less than 1 which is not a good assumption if $X_{Go}$ and $X_{Lo}$ are on the order of 0.1 as is the case here. To relax this assumption, Eq. [25] and [34] were solved by using Newman's numerical technique (5, 7) for the fixed and variable parameters considered here as shown in Table I (see Table II for a typical set of calculated parameter values).

Figure 3 shows a comparison between the predicted mol fraction distributions for the simplified and complete governing equations cases, and Fig. 4 presents a comparison of the predicted current densities for both cases. Also shown in Fig. 4 is the predicted limiting current density according to Austin (8, Eq. 6.38a)

$$i_L = \left(\frac{n\mathbf{F}D'_{GI}}{d}\right)\frac{X_{Go}P_o f}{RT} \quad [73]$$

where

$$f = \frac{\ln[(1 - X_{Go})^{-1}]}{X_{Go}} \quad [74]$$

**Table I. System parameters used for calculations**

| | |
|---|---|
| **Fixed Parameters** | |
| Gas phase | $X_{Go} = 0.21$ |
| Electrolyte | $X_{Lo} = 0.127$, $C = 0.05$ mol/cm³, $\gamma = 75$ dyn/cm, $\theta = 0°$ |
| Henry's law constant | $H = 3.99966 \times 10^{10}$ dyn/cm² |
| Porous medium characteristics | $\phi = 0.5$, $\tau = 15$, $d = 0.2$ cm, $\sigma = 5 \times 10^{-5}$ cm, $\bar{r} = 1.5 \times 10^{-4}$ cm, $a = 1.5 \times 10^4$ cm²/cm³ |
| Molecular diffusivities | $D_{GI} = 0.2$ cm²/s, $D_{LJ} = 2 \times 10^{-5}$ cm²/s, $D_{GJ} = 1 \times 10^{-5}$ cm²/s |
| Kinetic parameters | $n' = 4$, $\alpha = 1/2$, $i'_0 s = i_0/d$, $g' = 1.0$, $T = 298.15$ K |
| Stoichiometric coefficients | $g = 1$, $l = 4$, $n = 4$ |
| **Variable Parameters (with typical values)** | |
| Gas phase | $P_o = 1.6212 \times 10^6$ dyn/cm² |
| Kinetic parameters | $i_o = 10^{-5}$ A/cm², $l' = 1.0$, $\eta = 0.1$V |

**Table II. Calculated parameters for $g' = 1.0$, $i_o = 10^{-5}$ A/cm², $l' = 1.0$, $P_o = 1.6$ atm, and $\eta = 0.1$V**

| |
|---|
| $\phi_l = 0.4867$ |
| $\phi_g = 0.0133$ |
| $a_g = 2.29 \times 10^2$ cm²/cm³ |
| $K_G = 2.19$ |
| $K_L = 3.12$ |
| $K_A = 2.23 \times 10^{-6}$ A/cm² |

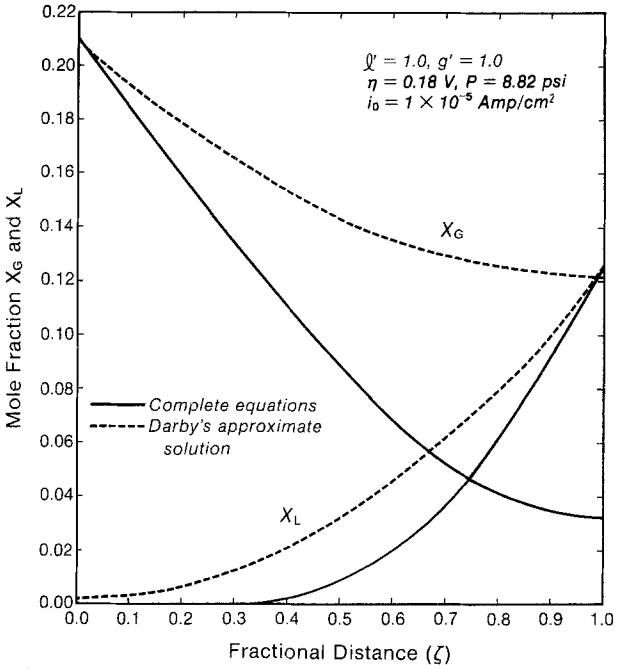


**Fig. 3. Mol fraction distributions for the complete governing equations model (Eq. [25] and [34]) with infinitely large $k_{mg}$ and $k_{ml}$, and Darby's approximate solutions (Eq. [68] and [69]) to the simplified governing equations (Eq. [66] and [67]).**

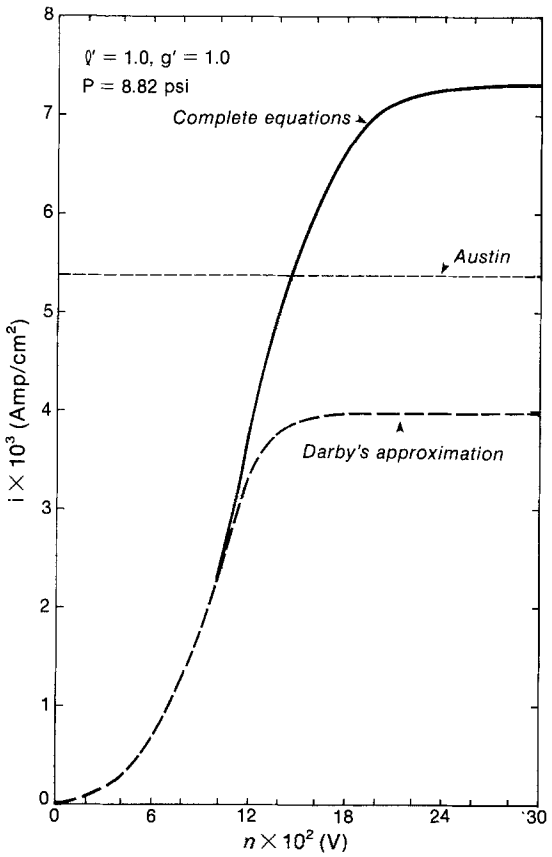


**Fig. 4. Comparison of predicted current densities by the complete model with infinitely large $k_{mg}$ and $k_{ml}$, Darby's approximate solutions, and Eq. [73] for the limiting current density with $i_o = 10^{-5}$ A/cm².**

Substitution of the appropriate values from Tables I and II into Eq. [73] and [74] gives $i_L = 5.27 \times 10^{-3}$ A/cm². Notice in Fig. 4 that for large values of $\eta$, the predictions of the complete model are significantly different from those of Darby's approximate solution. This is due to the importance of the neglected terms in the governing differential equations for the two cases (compare Eq. [25] and [66] and Eq. [34] and [67]). It is interesting that the prediction of the limiting current density by Austin's equation falls between these two cases. This is due to using an effective diffusion coefficient for oxygen ($D'_{GI}$) in Austin's equation which is the same as the effective diffusion coefficient ($D'_{GI}$) used in both of the other cases. If $D'_{GI}$ is determined by multiplying $D'_{GI}$ by $\phi/\tau$, instead of $\phi_g/\tau$, then the limiting current density predicted by Austin's equation is 37.6 (*i.e.*, $\phi/\phi_g$) times larger than that shown in Fig. 4.

The limiting current density for the complete model (as shown in Fig. 4) is plotted in Fig. 5 together with other limiting current density values at different differential pressures $P$. Also shown in Fig. 5 are the limiting current density predictions of Darby's approxi-

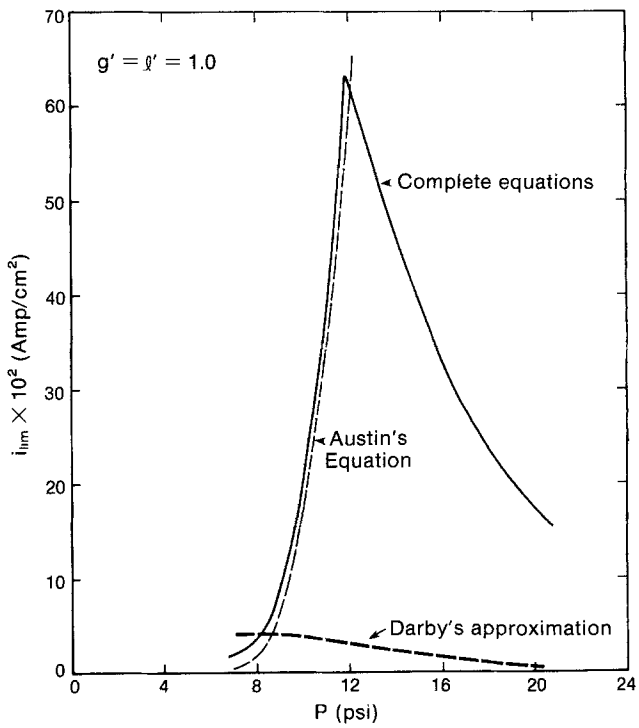


**Fig. 5. Limiting current density dependence upon $P$ for the complete model with infinitely large $k_{mg}$ and $k_{ml}$, Darby's approximate solution, and Eq. [73] with $i_o = 10^{-5}$ A/cm².**

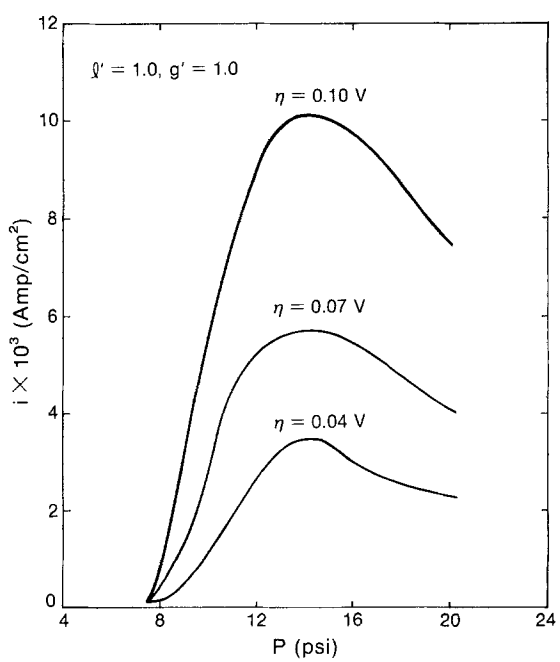


**Fig. 6. Predicted current density dependence on $\eta$ and $P$ for the complete model with infinitely large $k_{mg}$ and $k_{ml}$ where $i_o = 10^{-5}$ A/cm².**

mate solution and Eq. [73] again with $D'_{GI}$ determined with $\phi_g$ instead of $\phi$ (note that $\phi_g$ depends upon $P$). Figure 5 clearly shows that a maximum limiting current density is predicted at approximately $P = 12$ psi for the system considered here.

Figure 6 shows how the current density below the limiting current density depends on the differential pressure ($P$) for various values of $\eta$. Experimental current density values (3) have a similar dependence on $P$ and $\eta$ as shown in Fig. 7. Figures 6 and 7 are presented here for qualitative comparison only, since not enough information is available for a quantitative comparison between Darby's model and the experimental data presented in Fig. 7.

Figures 8 and 9 demonstrate how the kinetic parameters $l'$ and $i_o$ effect the predicted current densities. These figures show that predicted current densities depend upon these parameters to the extent that it should be possible to determine values for $l'$ and $i_o$ by comparison of data to predicted values using least squares, nonlinear fitting, for example.

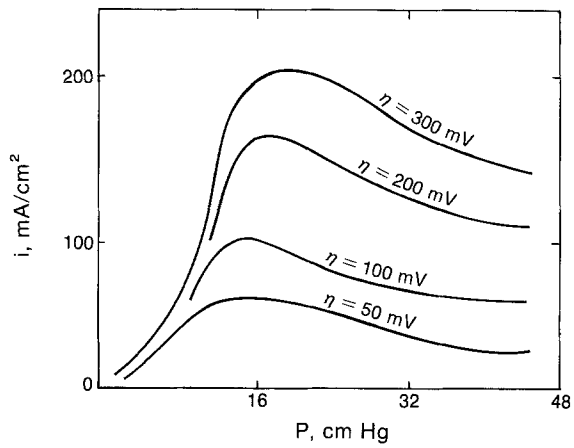


Fig. 7. Experimental current density (3) dependence on $\eta$ and $P$.

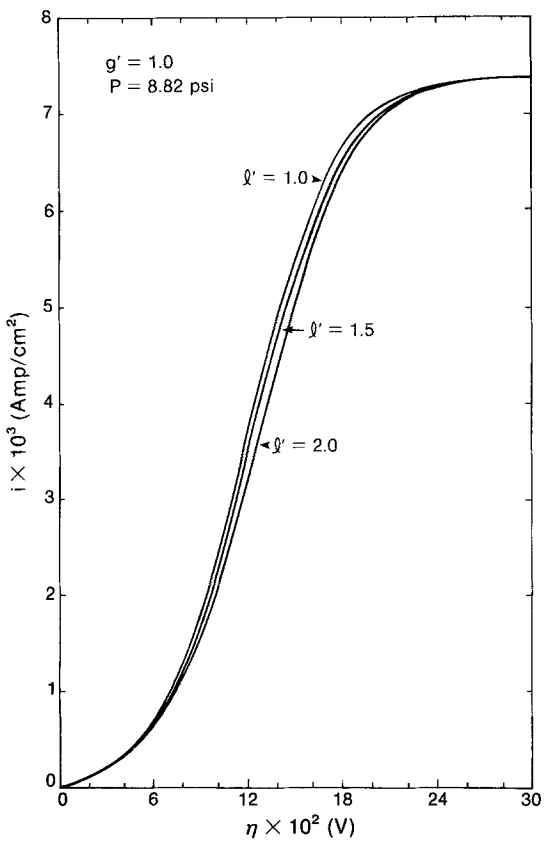


Fig. 8. Comparison of predicted current densities for various liquid reactant reaction orders for the complete model with infinitely large $k_{mg}$ and $k_{ml}$ when $i_o = 10^{-5}$ A/cm².

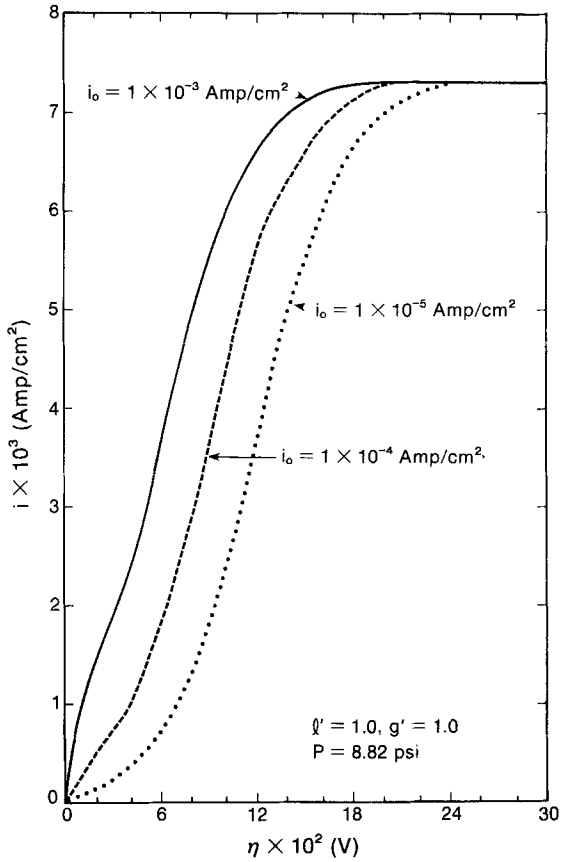


Fig. 9. Effect of the exchange current density on the predicted current densities for the complete model with infinitely large $k_{mg}$ and $k_{ml}$.

Finally, the effect of the external mass-transfer coefficients is demonstrated in Fig. 10 and 11. Figure 10 shows how the mass-transfer resistance to the electrode can alter the mol fraction distributions within the electrode, and Fig. 11 presents the effect of finite values of $k_{mg}$ and $k_{ml}$ on the predicted current density. Figure 11 clearly demonstrates that for large values of $\eta$ the predicted current density can be reduced significantly if external mass-transfer resistance of the reactants to the electrodes is important.

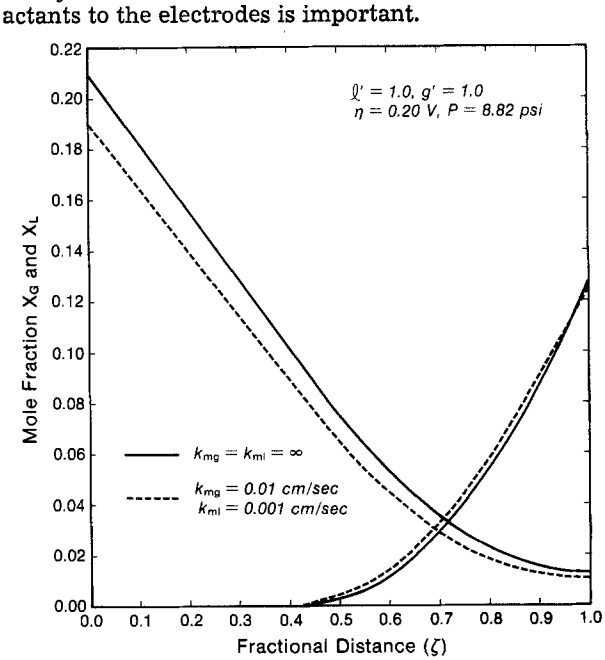


Fig. 10. Effect of external mass-transfer coefficients ($k_{ml}$ and $k_{mg}$) on the predicted mol fractions for the complete model when $i_o = 10^{-5}$ A/cm².

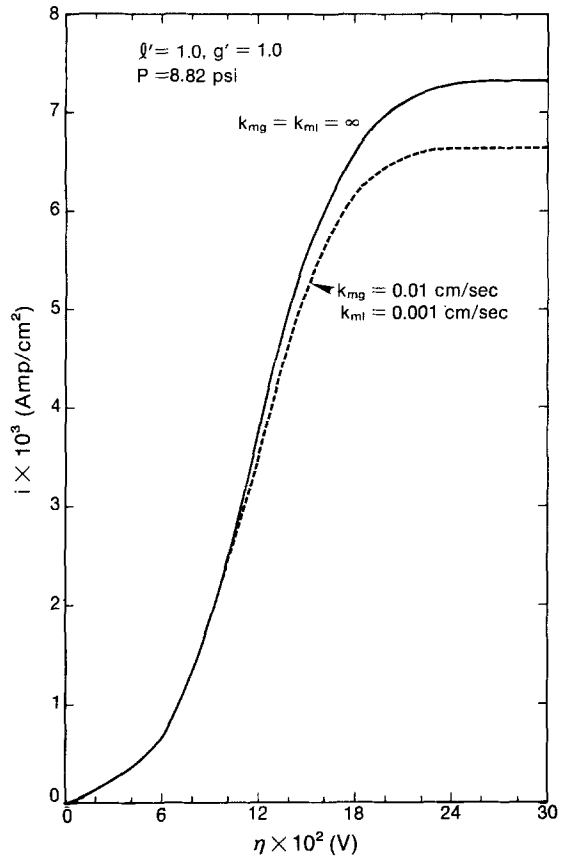


**Fig. 11. Effect of external mass-transfer coefficients ($k_{ml}$ and $k_{mg}$) on the predicted current densities for the complete model when $i_o = 10^{-5}$ A/cm².**

## Conclusion

Darby's model of a gas fed hydrophylic porous electrode is useful because it includes important features of hydrophylic porous electrodes which are often neglected. For example, it includes a pore size distribution for a porous electrode which can be determined experimentally and used in the model.

The extensions presented here (considering the complete governing equations, fractional reaction orders, and mass-transfer coefficients) should aid in data analysis and electrode design.

## Acknowledgments

The authors acknowledge gratefully the support of this work by the Dow Chemical Company.

Manuscript submitted March 18, 1983; revised manuscript received Sept. 13, 1983.

### LIST OF SYMBOLS

$a$ specific surface area, cm²/cm³
$a_g$ gas pore surface area per unit electrode volume, cm²/cm³
$C$ total liquid phase concentration, mol/cm³
$C_L$ concentration of liquid reactant, mol/cm³
$C_{Gi}$ concentration of the dissolved gas G at the gas-liquid interface, mol/cm³
$C_{Go}$ concentration of gaseous reactant at the gas-electrolyte interface at $z = 0$ (see Eq. [22]), mol/cm³
$d$ electrode thickness, cm
$D_{GI}$ diffusivity of the gas phase reactant in gas phase inert component, cm²/s
$D'_{GI}$ effective diffusivity of gas phase reactant in gas phase inert component in a porous medium, cm²/s
$D_{GJ}$ diffusivity of the gas phase reactant in liquid phase solvent, cm²/s
$D'_{GJ}$ effective diffusivity of the gas phase reactant in liquid phase solvent in a porous medium, cm²/s
$D_{LJ}$ diffusivity of liquid phase reactant in liquid solvent, cm²/s
$D'_{LJ}$ effective diffusivity of the liquid phase reactant in porous medium, cm²/s
$\mathbf{F}$ Faraday's constant, 96487C/mol
$f(r'_e)$ fraction of total pore volume in gas-filled pores (*i.e.*, cumulative pore size distribution for $r'_e$)
$g$ stoichiometric coefficient for gas phase reactant in overall electrode reaction
$g'$ reaction order with respect to gas phase reactant
$H$ Henry's law constant, dyn/cm²
$i$ current density, A/cm²
$i_o$ exchange current per unit of projected area of the electrode, A/cm²
$i'_o$ exchange current per unit of active catalytic surface area, A/cm²
$K_A$ parameter used to calculate $i$, A/cm²
$K_G$ dimensionless parameter for gas phase component
$K_L$ dimensionless parameter for liquid phase component
$k_{mg}$ gas phase mass-transfer coefficient, cm/s
$k_{ml}$ liquid phase mass-transfer coefficient, cm/s
$l$ stoichiometric coefficient for liquid phase reactant
$l'$ reaction order with respect to liquid phase reactant
$N_i$ molar flux of species i (i = G, J, I, L), mol/cm²-s
$n$ number of electrons involved in overall electrode reaction
$n'$ number of electrons in electrode reaction
$P$ differential pressure = $P_o - 1.01325 \times 10^6$ dyn/cm²
$P_G$ partial pressure of the gaseous reactant G, dyn/cm²
$P_o$ absolute gas pressure, dyn/cm²
$R$ gas constant, 8.3143J/mol-K
$r_e$ radius of a pore in which gas-liquid interface will be located, cm
$r'_e$ normalized radius of the largest flooded pore
$\bar{r}$ mean pore radius, cm
$\bar{r}_g$ mean pore radius of gas-filled pores, cm
$r'_g$ normalized mean pore radius of gas-filled pores
$s$ specific accessible catalytic surface area, cm²/cm³
$T$ absolute temperature, K
$X_G$ mol fraction of gas phase reactant
$X_{Go}$ mol fraction of gaseous reactant at the bulk phase-electrode interface ($\zeta = 0$)
$X_L$ mol fraction of liquid-phase reactant
$X_{Lo}$ mol fraction of liquid reactant-bulk phase ($\zeta = 1$)
$y$ depth into a liquid filled pore, normal to the gas-liquid interface, not in the same direction with respect to $z$ for all pores, cm
$z$ distance from the bulk gas-electrode interface into the porous electrode, cm

*Greek Symbols*

$\alpha$ transfer coefficient
$\alpha(r)$ pore size distribution, cm⁻¹
$\eta$ polarization (driving force), V
$\gamma$ surface tension of electrolyte, dyn/cm
$\phi$ porosity
$\phi_g$ porosity of gas-filled pores
$\phi_l$ porosity of liquid-filled pores
$\sigma$ standard deviation of pore size distribution function, cm
$\tau$ tortuosity
$\theta$ contact angle, degrees
$\zeta$ dimensionless coordinate, $z/d$

### REFERENCES

1. R. Darby, *Adv. Energy Convers.*, **5**, 43 (1965).
2. R. Darby, LTV Research Center Report 0-71000/34-26, Dallas, Texas (1963).
3. Yu. A. Chizmadzhev and Yu. G. Chirkov, in "Comprehensive Treatise of Electrochemistry," Vol. 6, E. B. Yeager, J. O'M. Bockris, B. E. Conway, and S. Sarangapani, Editors, p. 317, Plenum Press, New York (1983).
4. B. V. Tilak, R. S. Yeo, and S. Srinivasan, in "Comprehensive Treatise of Electrochemistry," Vol. 3,

J. O'M. Bockris, B. E. Conway, E. Yeager, and R. E. White, Editors, p. 39, Plenum Press, New York (1981).
5. J. S. Newman, "Electrochemical Systems," Prentice-Hall, Inc., Englewood Cliffs, NJ (1973).
6. D. B. Sepa, M. V. Vojnovic, and A. Damjanovic, *Electrochim. Acta*, **26**, 781 (1981).
7. R. E. White, *Ind. Eng. Chem. Fundam.*, **17**, 367 (1978).
8. L. G. Austin, in "Handbook of Fuel Cell Technology," C. Berger, Editor, Prentice-Hall, Inc., Englewood Cliffs, NJ (1968).

# Electrochemical Photocapacitance Spectroscopy Method for Characterization of Deep Levels and Interface States in Semiconductor Materials

**Ron Haak and Dennis Tench**

*Rockwell International Science Center, Thousand Oaks, California 91360*

ABSTRACT

The recently developed electrochemical photocapacitance spectroscopy (EPS) method for characterization of deep levels in semiconductors is described. Topics discussed include the advantages of the method, experimental considerations, and the determination of state densities and kinetic parameters (associated with state population/depopulation). Both steady-state and transient capacitance changes are treated mathematically. Data for n-GaAs, p-GaAs, n-CdSe, a-Si and p-$Zn_3P_2$ are presented to illustrate the wide applicability of the method and its sensitivity to both bulk and interface states, including those observed by other characterization methods.

Electrochemical photocapacitance spectroscopy (EPS) has recently been shown to be a sensitive means for characterization of deep levels in semiconductor materials (1). In the present paper, the EPS technique is described and illustrative results are presented for a variety of single-crystal and polycrystalline materials. Since the intent of the authors is to encourage and facilitate use of EPS by both physicists and electrochemists, considerable detail is given in areas expected to be unfamiliar to either group of scientists. It should also be emphasized that the focus here is on covering the practical aspects of applying the method rather than on providing a comprehensive quantitative treatment.

## EPS Method

In EPS, the capacitance of a reverse-biased semiconductor electrode is measured as a function of the wavelength of incident sub-bandgap light. The electrostatic situation and possible phototransitions for an n-type semiconductor are depicted in Fig. 1. In the dark, all of the negative charge in the electrolyte Helmholtz layer must be compensated by fixed ionized donors so that the space-charge layer extends deep into the semiconductor. At sufficiently anodic bias voltages (except at very high charge-carrier concentrations), the space-charge capacitance is generally small (<0.1 $\mu F/cm^2$) compared to the Helmholtz layer capacitance (~20 $\mu F/cm^2$). In this case, the impedance of the interfacial region is dominated by the space charge, so that additional charge, introduced by optical population/depopulation of traps or interface states, significantly affects the thickness of the space-charge layer and is readily detected as a change in capacitance. Transitions from bandgap states (electron traps) into the conduction band introduce additional fixed positive charge to the semiconductor space-charge region (or at the interface), reducing the thickness of the space-charge layer and increasing the capacitance. Similarly, transitions from the valence band to bandgap states (hole traps) result in a decrease in capacitance. Charge may also be introduced into the semiconductor space-charge region by localized transitions from the ground state to an excited state of an impurity (or defect center), followed by thermal injection of charge into one of the semiconductor bands (see Fig. 1). For p-type semiconductors, the capacitance change associated with a given type of transition is opposite in sign to that for an n-type material.

Typical plots of capacitance *vs.* wavelength (for sweeps from low to high photon energies) yield a series of plateaus and/or peaks, each corresponding to the population/depopulation of a given bandgap state. Plateaus are obtained for transitions that directly involve one of the semiconductor bands and can consequently be effected by light covering a wide range of energies above a certain threshold. Peaks are obtained for localized transitions which are effected only by light of a relatively specific energy. The onset energy of the capacitance change yields the energy of the state, relative to the appropriate bandedge. For localized transitions, the peak energy may be more de-

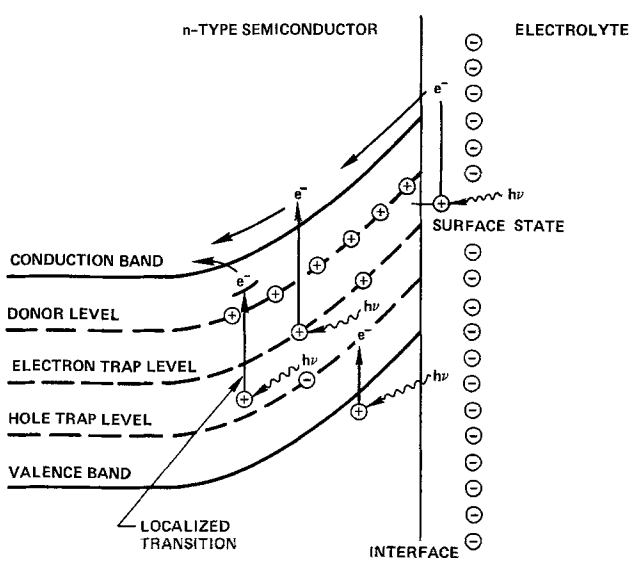


Fig. 1. Schematic representation of a reverse-biased n-type semiconductor, and typical phototransitions involved in electrochemical photocapacitance spectroscopy.

Key words: semiconductor traps, electrochemical detection, gallium arsenide, cadmium selenide, amorphous silicon, zinc phosphide.